Overcoming Ovarian Cancer Drug Resistance with a Cold Responsive Nanomaterial

Hai Wang,[†,‡,§] Pranay Agarwal,[‡,§] Gang Zhao,[∥] Guang Ji,[⊥] Christopher M. Jewell,[†,#,∇,○,◆] John P. Fisher,[†] Xiongbin Lu,[●] and Xiaoming He[*,†,‡,§,#,∇]

[†]Fischell Department of Bioengineering and [#]Robert E. Fischell Institute for Biomedical Devices, University of Maryland, College Park, Maryland 20742, United States

[‡]Department of Biomedical Engineering and [§]Comprehensive Cancer Center, The Ohio State University, Columbus, Ohio 43210, United States

[∥]Center for Biomedical Engineering, Department of Electronic Science and Technology, University of Science and Technology of China, Hefei, Anhui 230027, China

[⊥]Institute of Digestive Diseases, Longhua Hospital, Shanghai University of Traditional Chinese Medicine, Shanghai 200032, China

[∇]Marlene and Stewart Greenebaum Comprehensive Cancer Center, University of Maryland, Baltimore, Maryland 21201, United States

[○]Department of Microbiology and Immunology, University of Maryland School of Medicine, Baltimore, Maryland 21201, United States

[◆]United States Department of Veterans Affairs, Maryland VA Health Care System, Baltimore, Maryland 21201, United States

[●]Department of Medical and Molecular Genetics and Melvin and Bren Simon Cancer Center, Indiana University School of Medicine, Indianapolis, Indiana 46202, United States

S *Supporting Information*

ABSTRACT: Drug resistance due to overexpression of membrane transporters in cancer cells and the existence of cancer stem cells (CSCs) is a major hurdle to effective and safe cancer chemotherapy. Nanoparticles have been explored to overcome cancer drug resistance. However, drug slowly released from nanoparticles can still be efficiently pumped out of drug-resistant cells. Here, a hybrid nanoparticle of phospholipid and polymers is developed to achieve cold-triggered burst release of encapsulated drug. With ice cooling to below ~12 °C for both burst drug release and reduced membrane transporter activity, binding of the drug with its target in drug-resistant cells is evident, while it is minimal in the cells kept at 37 °C. Moreover, targeted drug delivery with the cold-responsive nanoparticles in combination with ice cooling not only can effectively kill drug-resistant ovarian cancer cells and their CSCs *in vitro* but also destroy both subcutaneous and orthotopic ovarian tumors *in vivo* with no evident systemic toxicity.

Conventional Sustained/Slow Drug Release

Cold-Triggered Burst Drug Release

Reduced pumping activity
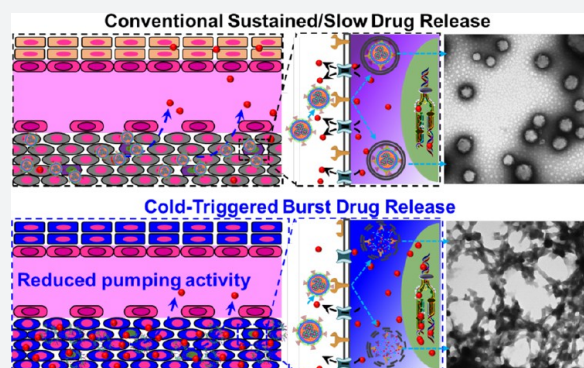
INTRODUCTION

Development of drug resistance in cancer cells is a major challenge to cancer chemotherapy.[1−3] Research on the mechanisms of drug resistance is usually focused on drug metabolism including its uptake, efflux, and detoxification.[1,4] A major advance in the understanding of drug metabolism is the identification of the membrane transporter P-glycoprotein (P-gp) that could pump free drug out of cancer cells.[5−7] However, it is worth noting that multiple mechanisms contribute to cancer drug resistance.[8,9] A critical advance in this aspect is the finding of the subpopulations of cancer cells that are highly tumorigenic and drug resistant. These cancer cells are usually referred to as cancer stem cells (CSCs) or tumor initiating/reinitiating cells.[10−12] There is mounting evidence showing that

the CSCs are responsible for cancer metastasis and tumor recurrence or relapse associated with conventional chemo-, radio-, and hormone therapies.[13−15] Several properties of the CSCs contribute to their high resistance to chemotherapeutic drugs including the overexpression of drug efflux pumps, enhanced DNA repair ability, overexpressed antiapoptotic proteins, and dormancy.[11,16,17] Therefore, it is important to account for the multiple mechanisms responsible for the drug resistance of cancer when developing strategies for effective cancer therapy.
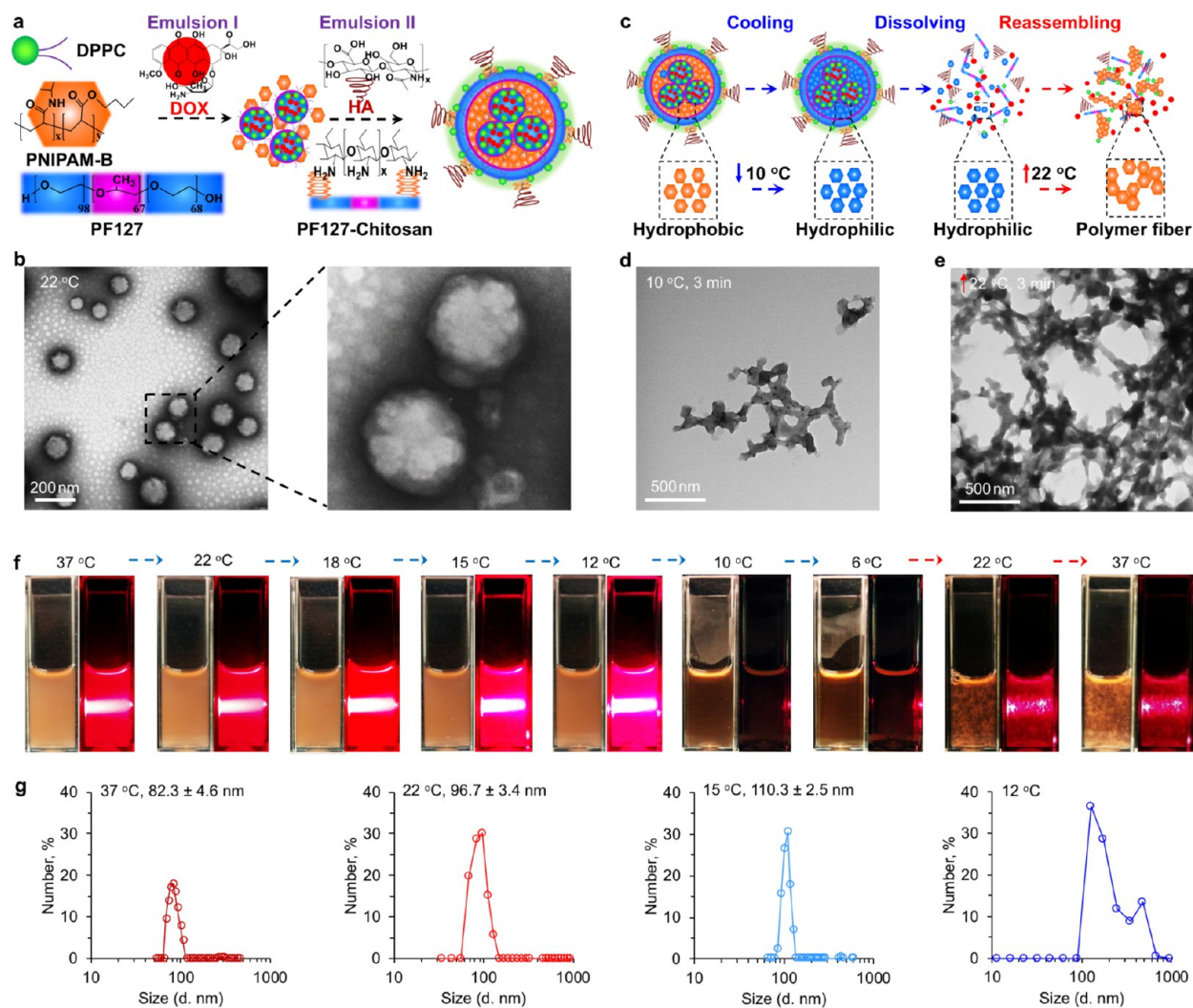
Figure 1. Synthesis and characterization of cold-responsive nanoparticle. (a) Hyaluronic acid (HA or H), lipid (dipalmitoylphosphatidylcholine or DPPC in this study, L), Pluronic F127 (PF127, P), poly(*N*-isopropylacrylamide-*co*-butyl acrylate) (PNIPAM-B or N), and chitosan (C)-modified Pluronic F127 (PF127-chitosan) were used to prepare the doxorubicin (DOX, D) laden HCLPN-D nanoparticles using the double-emulsion method. (b) TEM images showing the HCLPN-D nanoparticles are spherical with a multicore–shell configuration. (c) The thermally induced phase transition behavior of PNIPAM-B from being water-insoluble to highly water-soluble, which can cause disassembly of the HCLPN-D nanoparticles upon cooling to below room temperature. This can result in burst release of the encapsulated drug. (d) TEM images showing the HCLPN-D nanoparticles become completely disassembled after 3 min incubation at 10 °C. (e) An extensive network of polymer fibers rather than nanoparticles is observable after warming back to 22 °C. (f) Photographs of the aqueous samples of HCLPN-D nanoparticles at various temperatures before and after shining a red laser beam through them in the dark. As a result of the Tyndall effect (i.e., scattering of laser beam by nanoparticles in solution), a bright white track of light is visible in the dark in the solutions of HCLPN-D nanoparticles above 10 °C. However, it is not clearly observable at or below 10 °C and after warming back to 22 or 37 °C, indicating the HCLPN-D nanoparticles disassemble upon cooling to 10 °C (or a lower temperature), and the disassembling process is not reversible. (g) Size distribution of HCLPN-D nanoparticles measured by dynamic light scattering (DLS) at different temperatures. The results show a narrow size distribution of the HCLPN-D nanoparticles at 37, 22, and 15 °C. An additional peak of large particles is seen at 12 °C, probably due to aggregation of polymers. No stable peak of nanoparticles can be detected when the temperature is decreased to 10 and 6 °C.

Nanoparticle-based drug delivery systems have been explored for reducing the side effect of chemotherapeutic drugs as well as overcoming drug efflux pump-associated drug resistance.[18−22] The latter is because nanoparticles can be actively taken up by drug-resistant cancer cells via endocytosis instead of passive diffusion across the plasma membrane. Consequently, the drug encapsulated in nanoparticles can bypass the efflux pumps on the cell plasma membrane and enter the inner cytoplasm.[23] However, the function of the drug efflux pumps is not compromised during the uptake of the nanoparticles, and they can still pump out the drug slowly released from the nanoparticles in cells. Therefore, it may be important to

achieve burst release (i.e., release in a short time of seconds or minutes) of a large amount of free drug inside cancer cells, so that a significant amount of free drug could bind with its target (e.g., DNA, RNA, or proteins) before its depletion by the efflux pumps, for overcoming drug resistance.

Stimuli-responsive nanoparticles hold great promise for controlling drug release inside cells.[24,25] However, drug release from most existing stimuli-responsive nanoparticles (mainly pH- and heat-responsive ones) may still occur over hours to days.[26,27] This slowly released drug could be easily depleted by the efflux pumps before it binds with its target in cells. Moreover, no study has been conducted to test the existing

stimuli-responsive nanoparticles for overcoming drug resistance using CSCs. More recently, cold and freezing-temperature treatments (e.g., cryosurgery, cryotherapy, cryoablation, and hypothermia) have been widely studied and used for treating various diseases including cancer.[28−34] Nonetheless, nanoparticles that are responsive to cold (i.e., lower than room temperatures) have never been reported, although there are studies on nanoparticles responsive to temperatures higher than room temperature but blow body temperature.[35−37] Furthermore, the use of cold and nanoparticle drug delivery for overcoming cancer drug resistance has never been explored in the literature.

In this work, we developed a cold-responsive nanoparticle that quickly disassembles upon ice cooling, leading to burst release of most of the encapsulated chemotherapeutic drug (doxorubicin hydrochloride or DOX) in seconds. Moreover, the NCI/RES-ADR multidrug-resistant cancer cells (human ovarian cancer cells that were called MCF-7/ADR cells in early studies) and their CSCs together with A2780ADR drug resistant ovarian cancer cells, were used in this study to demonstrate the capability of overcoming cancer drug resistance with the cold-responsive nanoparticle *in vitro* and *in vivo*.

■ RESULTS

Preparation and Characterization of Nanoparticles. As shown in Figure 1a, the cold-responsive nanoparticles were prepared with the double-emulsion method using dipalmitoyl-phosphatidylcholine (DPPC) and four different polymers including Pluronic F127 (PF127), poly(*N*-isopropylacryla-mide-*co*-butyl acrylate) (PNIPAM-B, NIPAM:B = 8:1, M_n = 30,000), chitosan-modified PF127 (PF127-chitosan), and hyaluronic acid (HA). All four polymers have been widely used for various biomedical applications and are considered as biocompatible biomaterials, and PF127, chitosan, and HA have been approved by the Food and Drug Administration (FDA) for medical use.[38−41] PF127 is an amphiphilic polymer consisting of hydrophilic polyethylene glycol (PEG) blocks and more-hydrophobic polypropylene glycol (PPG) blocks.[35] The PNIPAM-B is a thermally responsive polymer with a lower critical solution temperature (LCST) of 14−16 °C, which means the polymer is insoluble in water (hydrophobic) at room temperature (~22 °C), while it is highly soluble in water (hydrophilic) at or below 14 °C.[42] DPPC is used to improve the biocompatibility of the nanoparticles.[43,44] First, aqueous solution containing DOX was emulsified with organic solvent containing PF127, PNIPAM-B, and DPPC. This leads to the formation of a water-in-oil structure to encapsulate DOX in the hydrophilic core dispersed in organic solvent (Figure 1a). For second emulsion, the product of the first emulsion is emulsified with the aqueous solution of chitosan-PF127 and HA. The hydrophobic part of chitosan-PF127 could integrate into the hydrophobic inner layer, while the hydrophilic part of chitosan-PF127 could bind with HA at the outermost layer of the resultant nanoparticles.[43,45] The reason to decorate HA on the surface of the nanoparticles is that HA is a natural ligand of the variant CD44 commonly overexpressed on many types of cancer cells and particularly CSCs.[46−48] Therefore, the surface of the nanoparticles consists mainly of PEG and HA, which makes the nanoparticles highly dispersible in aqueous solutions as both PEG and HA are hydrophilic. The nanoparticles can be collected by centrifugation after removing organic solvent by rotary evaporation under a vacuum.

Typical transmission electron microscopy (TEM) image of the resultant nanoparticles (HCLPN-D, H for HA, C for chitosan, L for the lipid DPPC, P for PF127, N for PNIPAM-B, and D for DOX) is shown in Figure 1b. The nanoparticles are ~100 nm in diameter with a spherical morphology, and interestingly, they have a multicore—shell structure. The multicore—shell structure is probably mainly due to the presence of lipid during the first emulsion when the lipid together with PNIPAM-B and PF127 may form small sized water-in-oil (W-in-O) structures. A few of them together may form the final nanoparticles after the second (W-in-O)-in-W emulsion. This is because the multicore—shell structure is not obvious for nanoparticles prepared in the same way without lipid (Figure S1). Moreover, few nanoparticles could be collected by centrifugation if PF127 and DPPC (PF127 + DPPC) were used for synthesizing nanoparticles using the same procedure (Figure S2a). Although more nanoparticles could be collected if PNIPAM-B and DPPC (PNIPAM-B +DPPC) were used, the drug encapsulation efficiency (EE) is lower than that of HCLPN nanoparticles (Figure S2b, 4.7 ± 2.5% for PF127 + DPPC, 14.5 ± 2.2% for PNIPAM-B+DPPC, and 59.7 ± 4.3% for HCLPN nanoparticles). This can be confirmed visually by the redness (the color of DOX) of the three different samples after removing nonencapsulated DOX by centrifugation and resuspending in deionized (DI) water (Figure S3a). When a red laser beam was shined through the three samples, the light track is weak in the PF127 + DPPC sample while it is evident in the PNIPAM-B + DPPC and HCLPN-D samples (Figure S3b) as a result of the Tyndall effect due to light scattering by nanoparticles. The TEM image of the PF127+DPPC sample shows that most of the DPPC form liposomes during the preparing process (Figure S3c). Although core—shell nanoparticles are formed in the PNIPAM-B + DPPC sample, their size is not uniform, and some can be as big as ~400 nm in diameter (Figure S3d).

Cold-Responsiveness of HCLPN-D Nanoparticles. We next investigated the cold-responsive property of the HCLPN-D nanoparticles. As aforementioned, the PNIPAM-B polymer for making the nanoparticles is hydrophobic at room temperature and has an LCST of 14−16 °C. Once the temperature is lower than the LCST, the PNIPAM-B polymer becomes water-soluble. This may cause disassembly of the nanoparticles in aqueous solutions (Figure 1c). Indeed, almost all the HCLPN-D nanoparticles were disassembled after incubating at 10 °C for 3 min (Figure 1d). Extensive polymer aggregates formed when the temperature was increased back to room temperature (22 °C, Figure 1e). This is further confirmed by shining a red laser beam through the aqueous samples of the HCLPN-D nanoparticles at different temperatures. A light track in the sample indicates the presence of nanoparticles. As shown in Figure 1f, the aqueous solution of the nanoparticles appears homogeneous at both 37 and 22 °C before cooling. This is attributed to the high dispensability of the nanoparticles in aqueous solutions. When the temperature decreases to 10 or 6 °C, the solution of HCLPN-D nanoparticles becomes transparent, and no evident light track could be observed, suggesting disassembly of the nanoparticles and dissolution of polymers in the nanoparticles in the aqueous solution. More importantly, many visible polymer aggregates formed when the temperature was increased back to room or body temperatures (22 and 37 °C respectively, Figure 1f), suggesting the disassembly is irreversible. We further checked the size distribution of HCLPN-D nanoparticles at different temperatures by dynamic
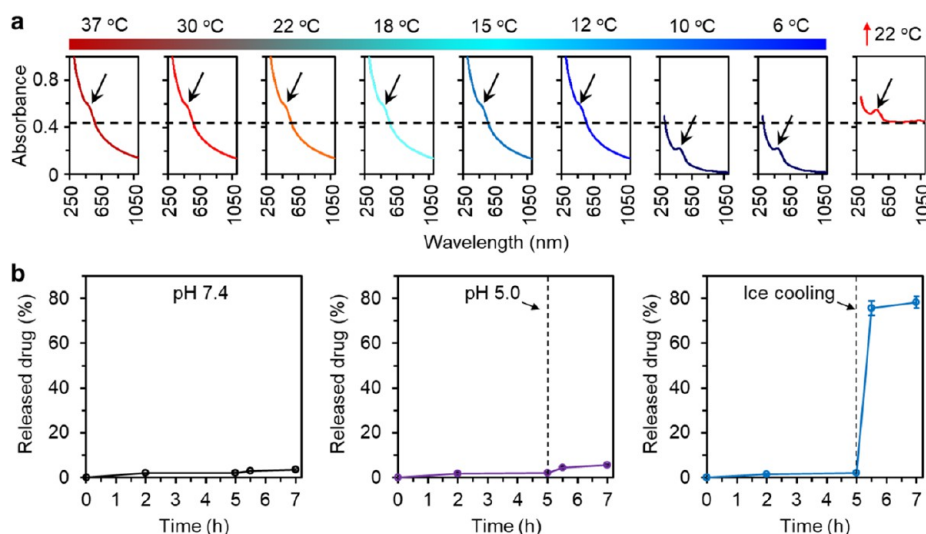
Figure 2. Cold-triggered burst drug release from HCLPN-D nanoparticles. (a) UV−vis absorbance of HCLPN-D nanoparticles at different temperatures showing the cold-responsiveness of HCLPN-D nanoparticles. Arrows indicate the absorbance peaks of DOX. (b) A comparison of the release of DOX from HCLPN-D nanoparticles under pH 7.4, acidic pH (5.0, 5 min), and ice cooling (5 min), showing the cold temperature is much more effective than low pH in triggering drug release from the HCLPN-D nanoparticles. Error bars represent ± standard deviation (SD, $n = 3$).

light scattering (DLS). The HCLPN-D nanoparticles have a narrow size distribution with one single peak at temperatures of 37, 22, and 15 °C (82.3 ± 4.6, 96.7 ± 3.4, and 110.3 ± 2.5 nm in diameter, respectively), but a second peak of much larger particles/aggregates appears at 12 °C (Figure 1g). Moreover, no stable measurement could be made at 10 and 6 °C, probably because nearly all the nanoparticles are dissembled at the cold temperatures. The stability of HCLPN-D nanoparticles in acidic solution (pH 6.5) was further checked as the tumor microenvironment is often acidic with a pH value of ∼6.5.[49] As shown in Figure S4, the size distribution measured by DLS suggested the HCLPN-D nanoparticles are stable at pH 6.5. However, the nanoparticles are not stable at pH 5.0 (the pH value of late endosomes and lysosomes) as their size increases and even form some aggregates of ∼2.5 μm in pH 5.0 solution. Lastly, the HCLPN-D nanoparticles are stable at room temperature for at least 49 days according to the DLS size analyses (Figure S5).

We further checked the ultraviolet−visible (UV−vis) absorbance of the HCLPN-D nanoparticles at different temperatures. As shown in Figure 2a, the absorbance peak (arrow) of DOX at 486 nm is not obvious at or above 12 °C due to the strong absorbance of the HCLPN nanoparticles at the same wavelength. However, it shows up more clearly at 10 or 6 °C because of dissolution of polymers in the nanoparticles. When the temperature increased back to 22 °C, the absorbance is strong at all wavelength. This suggests the polymer aggregates may block the light to result in the strong absorbance. To confirm this, the drug release profile of HCLPN-D nanoparticles was determined by using ice to cool the samples. The drug release from HCLPN nanoparticles is slow at 37 °C (∼2.2% in 5 h), while more than 70% of DOX can be released from the nanoparticles after cooling on ice for 5 min (Figure 2b). In contrast, the drug release is less than 5% if the nanoparticles are kept at low pH (5.0) for 5 min. These drug release data indicate that cold is an effective stimulus for triggering drug release from the HCLPN nanoparticles, and it is much more efficient than pH excursion.

Overcoming Drug Resistance and Cancer Targeting *in Vitro*. Both two-dimensional (2D) cultured NCI/RES-ADR multidrug-resistant cancer cells and three-dimensional (3D)-cultured CSC-enriched spheres (obtained by suspension culture of the NCI/RES-ADR cells in CSC medium in ultralow attachment plates) were used in this study. We confirmed the resistance to free DOX of the 2D cultured NCI/RES-ADR cells by incubating the cells with free DOX (10 μg/mL) for 3 h. As shown in the first row of Figures 3a and S6, no red fluorescence of DOX is observable in the 2D cultured NCI/RES-ADR cells. In stark contrast, red fluorescence of DOX is observable in the cells when they are incubated with the HCLPN-D nano-particles (Figures 3a and S7). However, DOX is predominantly distributed in the cytosol, and it is barely observable in the nuclei of the NCI/RES-ADR cells incubated with the HCLPN-D nanoparticles. Since DOX has to enter the nuclei for cytotoxicity, the data suggest that simply using nanoparticles for uncontrolled drug release may not be able to efficiently overcome the drug resistance of the NCI/RES-ADR cells. To check if cold-triggered burst drug release could overcome the drug resistance, the cells treated with free DOX or HCLPN-D nanoparticles for 3 h were further cooled with ice for 5 or 10 min. For the cells treated with free DOX, the red fluorescence is still not observable (Figure 3a and Figure S6). Interestingly, DOX is located in part of the nuclei of the cells treated with HCLPN-D nanoparticles after cooling for 5 min, and DOX overlaps with nearly all the nuclei after 10 min of cooling (Figure 3a and Figure S7). In contrast, almost all DOX is still distributed in the cytosol if the cells are continuously cultured at 37 °C, indicating the cold-triggered burst drug release indeed can overcome the drug-resistant capacity of the NCI/RES-ADR cancer cells.

In order to confirm the temperature drop to below 12 °C in the cells with ice cooling, FLIR (Wilsonville, Oregon, USA) near-infrared thermography was used to determine the temperature of the samples. As illustrated in Figure S8, the temperature of samples treated with free DOX or HCLPN-D nanoparticles is ∼37 °C in incubator, decreases to ∼4−0 °C (within ∼3 min) after ice cooling for 5 or 10 min, and returns
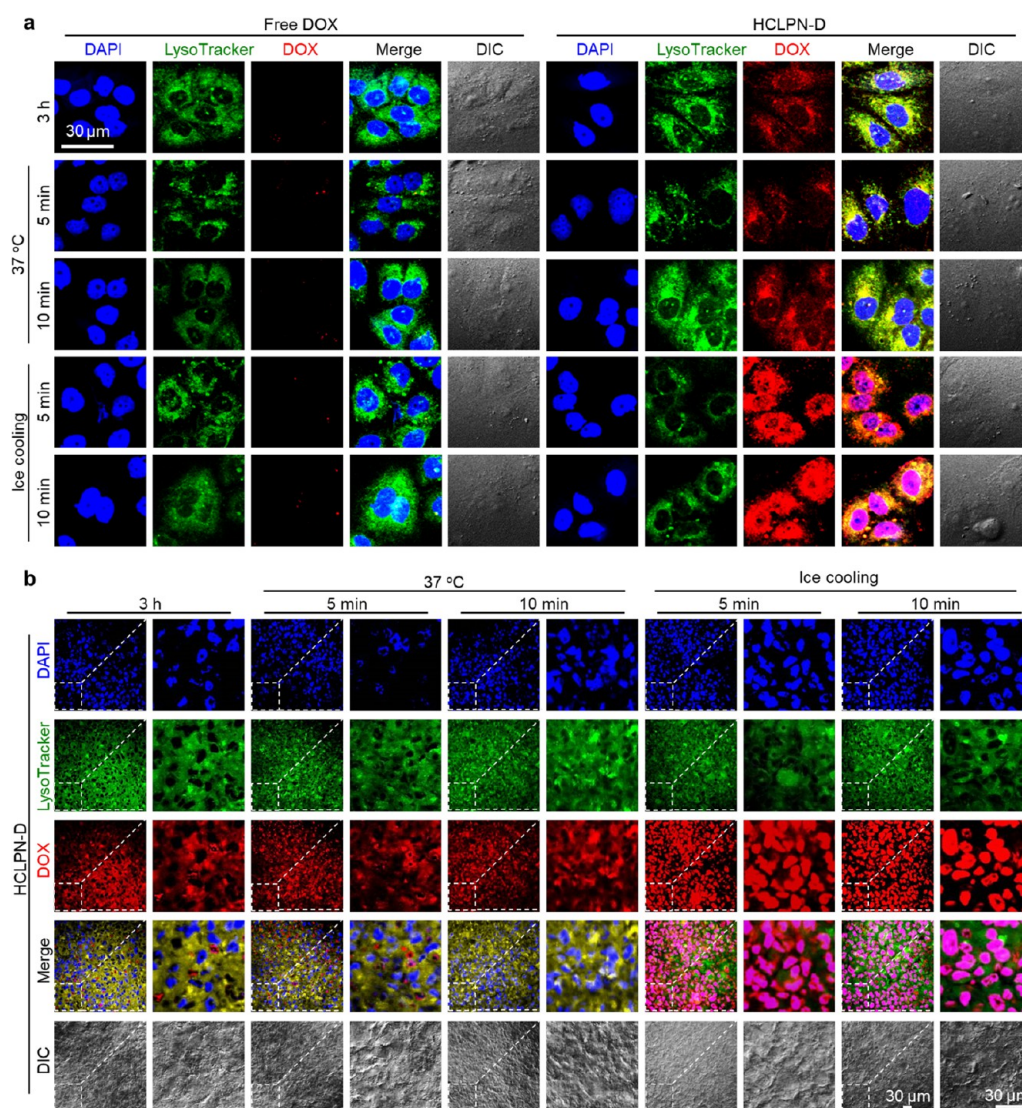
Figure 3. Overcoming cancer drug resistance with cold-triggered burst drug release form HCLPN-D nanoparticles. (a) Confocal micrographs of 2D cultured NCI/RES-ADR multidrug-resistant cancer cells after incubating them with either free DOX or HCLPN-D nanoparticles for 3 h at 37 °C, followed by either continued culturing in incubator (37 °C) or ice cooling (+I) for 5 or 10 min. (b) Confocal images of CSC-enriched spheres derived from the multidrug-resistant cancer cells after incubating them with HCLPN-D nanoparticles for 3 h at 37 °C, followed by either continued culturing in incubator (37 °C) or ice cooling (+I) for 5 or 10 min. DOX could enter the cell nuclei only when treated with both HCLPN-D nanoparticles and ice cooling, indicating the cold-triggered burst drug release from the HCLPN-D nanoparticles could be used to overcome the drug resistance of the 2D cultured cancer cells and their CSCs.

to ~37 °C after warming in incubator for 5 min. This is consistent with the medium temperature in the sample measured with thermocouples (Figure S9).

It is also noticeable that the overall fluorescence intensity of DOX inside cells after ice cooling increases compared with cells kept at 37 °C, probably due to the following three reasons. First, the fluorescence intensity of DOX decreases after encapsulated inside the nanoparticles due to self-quenching (Figure S10). After ice cooling, the free DOX released from the HCLPN-D nanoparticles results in higher fluorescence intensity. Second, the fluorescence intensity of DOX decreases slightly in acidic solution (Figure S10). HCLPN-D nanoparticles are taken up by cells via endocytosis and locate inside the endo-/lysosomes (pH ≈ 5.0). The fluorescence intensity of DOX should increase after the DOX is released from the nanoparticles and enter the nuclei with a pH value of ~7.0. Third, the high binding affinity of DOX with cell nuclei may

lead to accumulation of DOX in the cell nuclei, which should result in increased fluorescence.[50]

CSC-enriched spheres were also treated in the same way as that aforementioned for 2D cultured cells. Similarly, the CSC-enriched spheres are resistant to free DOX, but can take up the HCLPN-D nanoparticles (Figures S11 and 3b). Importantly, most of the DOX can enter the cell nuclei after cooling the spheres with ice for 5 or 10 min. Further quantitative analyses show that the intensity of DOX in cell nuclei is significantly increased after ice-cooling (Figure S12). Next, we investigated the cellular uptake of different concentration (5, 10, and 25 μg/mL) of free DOX or HCLPN-D nanoparticles with or without ice cooling for 10 min. As shown in Figures S13−16 (Figures S13−14 for free DOX and Figures S15−16 for HCLPN-D nanoparticles), no red fluorescence of DOX is observable in the multidrug-resistant cells treated with free DOX, while more DOX could be observed in cells treated with high concentration
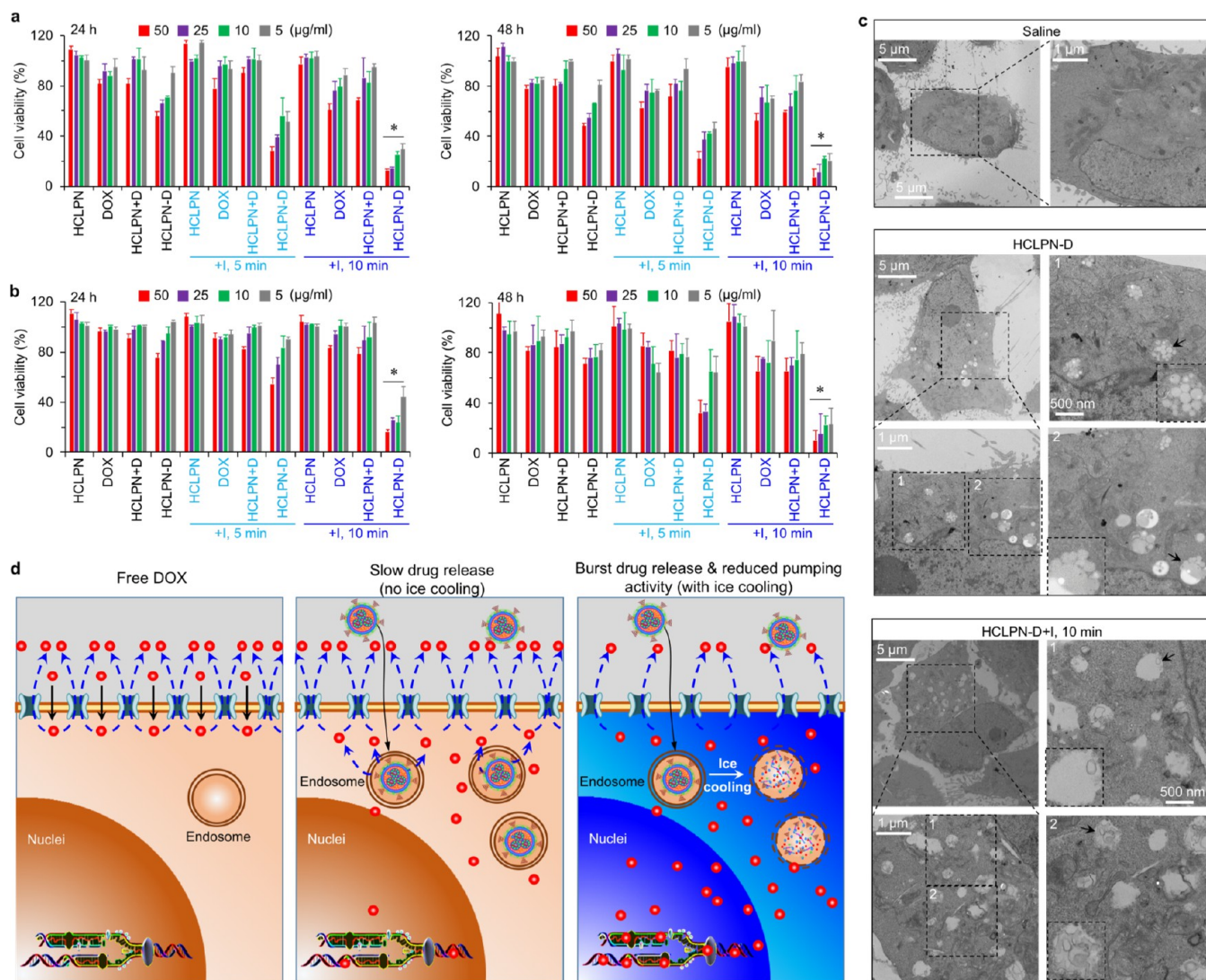
571

Figure 4. Enhanced *in vitro* anticancer capacity by HCLPN-D nanoparticles with ice cooling for overcoming drug resistance. Viability of (a) 2D cultured NCI/RES-ADR multidrug-resistant cancer cells and (b) CSC-enriched spheres derived from the multidrug-resistant cancer cells after treating them with blank nanoparticles (HCLPN), free DOX, and HCLPN-D nanoparticles without or with ice cooling for 5 or 10 min. The viability of control cells cultured in pure medium is 100%. Error bars represent SD ($n = 3$). *: $p < 0.05$ (Kruskal−Wallis H test), which indicates cells treated with HCLPN-D nanoparticles and ice cooling for 10 min is significantly lower than other treatments with the same drug concentration. (c) TEM images of the NCI/RES-ADR cancer cells treated with saline, HCLPN-D nanoparticles with or without ice cooling for 10 min. The endo-/lysosomes in HCLPN-D treated cells light up due to the existence of intact (without ice cooling) or disassembled (with ice cooling) HCLPN-D nanoparticles. The insets are the endo-/lysosomes indicated by the arrows with either intact or disassembled HCPN-CG nanoparticles. (d) A schematic illustration of the combination of the HCLPN-D nanoparticle and ice cooling for overcoming the multidrug resistance to enhance cancer destruction, in comparison to the HCLPN-D nanoparticle alone and free drug. The combination can overcome the drug resistance in cancer cells by (1) cold-triggered burst drug release from the HCLPN-D nanoparticles and (2) the cold-induced low activity of the membrane transporters to pump out the released drug.

of HCLPN-D nanoparticles. After ice cooling, stronger fluorescence is observable in the cells treated with HCLPN-D nanoparticles, particularly at high concentrations. This is not observable for free DOX treated cells. Similarly, quantitative analysis of DOX in the cell nuclei reveals that cells treated with HCLPN-D nanoparticles and ice cooling have higher DOX concentration in their nuclei (Figure S17). Since the pH value of the tumor microenvironment is ∼6.5, we checked the capacity of overcoming drug resistance by the HCLPN-D nanoparticles at pH 6.5. As shown in Figure S18, most of the DOX released from the HCLPN-D nanoparticles as a result of ice cooling enters the nuclei of cancer cells both under 2D culture and in CSC-enriched spheres, suggesting the HCLPN-

D nanoparticles can still be used to overcome cancer drug resistance in the acidic tumor microenvironment.

As the HA modified on the surface of HCLPN-D nanoparticles is used to target CD44, we first studied the expression of CD44 on the 2D cultured NCI/RES-ADR cells and cells in the CSC-enriched spheres by using flow cytometry. As shown in Figure S19a,b, the expression of CD44 on the NCI/RES-ADR cells is positive, and it is similar to that on MDA-MB-231 cancer cells that are considered as CD44 positive.[51,52] Moreover, the expression of CD44 on cells in the CSC-enriched spheres is significantly higher than that on the 2D cultured NCI/RES-ADR cells, suggesting the HCLPN-D nanoparticles can be used for targeting both the drug-

resistant cancer cells and their CSCs. The data also demonstrate that CSCs are enriched in the 3D cultured NCI/RES-ADR spheres because CD44 is a common CSC marker.[47,48,53] Furthermore, the binding between the nanoparticles with HA on their surface and CD44 is confirmed using confocal fluorescence microscopy. As shown in Figure S20, most of the CD44 in control group is located on the surface of the cell membrane. Moreover, many of them are internalized into the cytoplasm after incubated with the HCLPN-D nanoparticles, suggesting the nanoparticles bind with CD44 and are then taken up by the cells. Interestingly, some line structures with CD44 are observable after ice cooling. This is probably because polymers bound with CD44 on the surface of the HCLPN-D nanoparticles could form fibers after cooling-induced disassembly of the nanoparticles (Figure 1e). The targeting capability of HCLPN-D nanoparticles was further confirmed by treating the drug resistance cells using nanoparticles without HA modification on their surface (LPN-D). As shown in Figure S21a, more DOX could be delivered inside the cells with HCLPN than LPN nanoparticles due to the targeting capability of HA on the HCLPN nanoparticles. Therefore, after cooling with ice, the HCLPN-D nanoparticles can be used to deliver more DOX into the nuclei than LPN-D nanoparticles (Figure S21b).

Enhanced Anticancer Capacity *in Vitro* via Overcoming Drug Resistance. To investigate the anticancer capacity of HCLPN-D nanoparticles, both the 2D drug-resistant cancer cells and 3D CSC-enriched spheres were treated with HCLPN nanoparticles (without DOX), free DOX, and HCLPN-D nanoparticles at various concentrations without or with ice (+I) cooling for 5 or 10 min. The total treatment time for all the drug formulations is either 24 or 48 h. For treatments with ice cooling, it was conducted after incubating cells with the various formulations at 37 °C for 12 h, and the cells were put back in 37 °C incubator after the cooling treatment to further culture for 12 or 36 h. FLIR thermographs indicate that cells cultured in a 96-well plate can be efficiently cooled to ~4−0 °C with ice for 5 or 10 min (Figure S22a), which is consistent with the medium temperature in the sample measured with thermocouples (Figure S22b). The safety of ice treatment is confirmed by checking the viability of cells incubated with ice for 5 or 10 min. As shown in Figure S23, the ice treatment alone has no effects on the cell viability at both 24 and 48 h. According to the viability data of both 2D cultured NCI/RES-ADR cells (Figure 4a) and CSC-enriched spheres (Figure 4b), blank HCLPN nanoparticles with or without ice cooling are also not harmful to the cells for both the 24 and 48-h treatments. Interestingly, HCLPN-D nanoparticles show higher cytotoxicity than free DOX only at high drug concentrations (50, 25, and 10 μg/mL for 2D cells; 50 μg/mL for CSC-enriched spheres, $p < 0.05$), probably due to the capability of the membrane transporter to pump out drug slowly released from the nanoparticles. However, the cytotoxicity of DOX is not significantly affected if it is simply mixed with blank HCLPN nanoparticles with or without ice cooling. In addition, ice cooling for 10 min could further significantly decrease the viability of 2D cells or spheres treated with free DOX at 50 μg/mL ($p < 0.05$, for both 2D cultured NCI/RES-ADR cells and CSC-enriched spheres). This is probably due to the reduced activity of membrane transporters in the cells cooled with ice for 10 min, which may allow some free DOX to enter the cells treated with free DOX at the high concentration. To confirm this, we further checked the uptake

of free DOX at high concentrations (50, 80, and 160 μg/mL) under the same thermal treatments for obtaining the data in Figure 3. As shown in Figure S24, although some free DOX could enter the drug-resistant cells at 50 μg/mL, it is minimal in the cell nuclei. This may explain the high viability of the cells treated with 50 μg/mL free DOX (Figure 4a). The fluorescence intensity gradually increases at higher drug concentrations. Although ice cooling for 5 min does not seem to significantly improve the intracellular DOX at all the three concentrations (Figure S24), significantly more DOX could enter the cells with ice cooling for 10 min. The latter is probably because the membrane transporter activity of the cells is significantly decreased after 10 min of ice cooling.

It is worth noting that most of the DOX remains in the cytoplasm after entering the drug-resistant cells incubated with the free DOX at the usually high concentrations, although free DOX usually enter the nuclei of non-drug-resistant cancer cells. This is further confirmed by incubating the cancer cells with free DOX on ice for 1 h. As shown in Figure S25, more free DOX could enter the cells compared to 5 or 10 min of ice cooling (Figure 3a). This suggests cold could decrease the activity of the efflux pump (i.e., temperature-dependent activity of the pump), but it requires more than 10 min for the activity to be sufficiently compromised for free DOX to enter the drug-resistant cells. Nonetheless, most of the free DOX stays in the cytoplasm after the 1 h of ice cooling, which is similar to the observation after incubating the cells with free DOX at high concentrations (50−160 μg/mL) on ice for 5−10 min (Figure S24). This may explain the cell viability data shown in Figure S26 because DOX must enter the cell nuclei to induce cytotoxicity. Although the toxicity of free DOX at 160 μg/mL to the drug-resistant cells with 10 min of ice cooling is significantly higher than that to the cells kept at 37 °C or with 5 min of ice cooling, more than 60% of the cells could still survive at such an unusually high concentration. These observations suggest the diffusion of free DOX through the plasma membrane into the drug-resistant cells may activate some protective mechanism to prevent the drug from entering the nuclei, in addition to trying to pump out the free drug with the membrane transporters.

In stark contrast, the cytotoxicity of HCLPN-D nanoparticles can be significantly enhanced after ice cooling (particularly for 10 min) at both low and high concentrations (Figure 4a,b), which is in accordance with the data on cellular uptake and DOX distribution in the cells (Figures 3 and S12). A higher cytotoxicity (~40 versus ~60%) could be achieved by using HCLPN-D+I (10 min) treatment with very low drug concentration compared with free DOX treatment (32 times lower, 5 versus 160 μg/mL). The cold-responsive capacity of HCLPN-D nanoparticles inside cells is further confirmed by cell TEM imaging. As shown in Figure 4c, although endo-/lysosomes are not easily identifiable in saline treated cells, they are lit up as white dots in cancer cells treated with the HCLPN-D nanoparticles. This is probably a result of the white core−shell structure of the nanoparticles under TEM (Figure 1b). Moreover, almost all the HCLPN-D nanoparticles in the endo-/lysosomes become disassembled after ice cooling, suggesting the cold-responsive capacity of the HCLPN-D nanoparticles retains inside cells. It is worth noting that disassembly of HCLPN-D nanoparticles with ice cooling partially disrupts the structure of endo-/lysosomes according to the TEM images. This could facilitate the DOX released from the nanoparticles to further escape from the endo-/
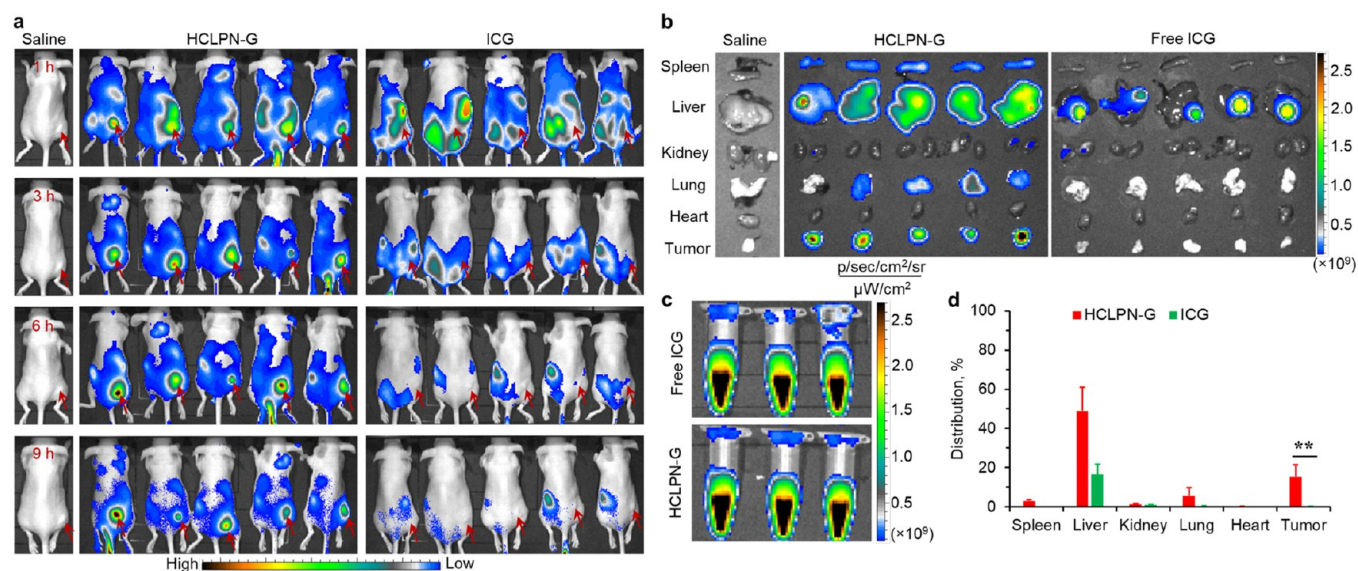
Figure 5. *In vivo* tumor targeting capacity of HCLPN-D nanoparticles. (a) *In vivo* whole animal imaging of ICG fluorescence at different times after intravenous injection of free ICG and ICG-laden HCLPN-G nanoparticles via the tail vein. Arrows indicate the locations of tumors in mice. (b) *Ex vivo* imaging of ICG fluorescence in tumor and five critical organs collected after sacrificing the mice at 9 h. (c) Imaging of total ICG fluorescence of free ICG and ICG-laden HCLPN-G nanoparticles in three samples prepared in the same way as the solutions used for injection into mice. The images were taken under the same condition as that for both the *in vivo* and *ex vivo* imaging. (d) Quantitative analysis of the distribution of HCLPN-G and free ICG in tumor and five critical organs collected from free ICG and HCLPN-D nanoparticles treated mice. The data show that the HCLPN-G nanoparticles could accumulate in tumor much more efficiently than free ICG. NCI/RES-ADR cells detached (with trypsin) from CSC-enriched spheres were used to obtain xenografts of multidrug-resistant tumors for imaging.

lysosomes into the cytoplasm. These data indicate that the aforementioned challenges associated with free DOX can be efficiently resolved by using the cold-responsive HCLPN-D nanoparticles for intracellular delivery of the drug (Figures 3 and 4).

We also incubated both 2D cultured cells and 3D CSC-enriched spheres with free DOX and loperamide, a substrate of P-gp and can be used as the P-gp inhibitor.[54] As shown in Figure S27, by mixing with P-gp inhibitor, free DOX indeed is significantly more toxic than the free drug alone (Figure 4a) to the 2D cultured cells after 24 h of incubation, and the cytotoxicity further increases at 48 h. For 3D CSC-enriched spheres, free DOX mixed with loperamide shows higher cytotoxicity than the free drug alone (see Figure 4b) only after 48 h of incubation. Moreover, the overall cytotoxicity of free DOX mixed with loperamide is still less than that of HCLPN-D nanoparticles with ice cooling (Figure 4a,b). This is probably because most of the free DOX and sustained/slowly released DOX from HCLPN-D nanoparticles (without ice cooling) may still stay in the cytoplasm after entering the cancer cells in the presence of loperamide to block the efflux pump. This hypothesis is confirmed with confocal images of cells treated with free DOX and HCLPN-D nanoparticles in the absence or presence of loperamide, as shown in Figure S28.

A schematic illustration of the combination of the HCLPN-D nanoparticles and ice cooling for overcoming the drug resistance to enhance cancer destruction, in comparison to the HCLPN-D nanoparticle alone and free drug, is given in Figure 4d. Free drug can be quickly pumped out of cells after its diffusion into cells due to its close proximity to the membrane transporters (or immobilized in the cytoplasm by possible additional mechanism when the drug concentration is unusually high). Using nanoparticles alone for slow drug release, the nanoparticles may be taken up by cancer cells via CD44 receptor-mediated endocytosis (Figure S20), which may also be mediated by clathrin or caveolin.[55,56] However, most of the slowly released drug may be still pumped out of the cells before it binds with its targets in the cells. This is because the activity of transmembrane transporters is intact, and the concentration of drug in cells is not high enough to outperform the pumping capacity of the transporters. Importantly, the HCLPN-D nanoparticles could quickly disassemble to release most of the encapsulated drug when cooled with ice and disrupt the structure of endo/lysosomes. Due to its small size, the released free DOX can diffuse out of the damaged endo-/lysosomes driven by its concentration gradient without the need of any metabolic energy. Although some of the released drug may be pumped out of cells during the cooling process, most of the drug can enter and bind with the nuclei due to the burst release-induced high drug concentration in the cytoplasm and the compromised pumping capacity of the transporters at cold temperature (Figure 4d).

***In Vivo* Tumor Targeting and Enhanced Capacity of Destroying Drug Resistant Tumors.** Next, we investigated the biodistribution of the HCLPN nanoparticles in drug-resistant tumor-bearing mice by encapsulating indocyanine green (ICG or G) to obtain ICG-laden nanoparticles (HCLPN-G). Tumors were produced by subcutaneous injection into the upper hindlimb of 20,000 CSC-enriched sphere cells per animal (7 week-old female nude mouse). As shown in Figure 5a, the ICG fluorescence was detectable over almost the whole animal body for both HCLPN nanoparticles and free ICG at 1 h after intravenous injection. More importantly, the HCLPN-G nanoparticles treated mice have stronger fluorescence in their tumors, suggesting preferential accumulation of the HCLPN nanoparticles in the tumors. The accumulation of HCLPN-G nanoparticles in tumor further increases after 3 and 6 h of injection. In contrast, the fluorescence in free ICG-treated mice decreases at 3 h and almost disappears at 6 h after injection (Figure 5a). To confirm the observations from whole animal
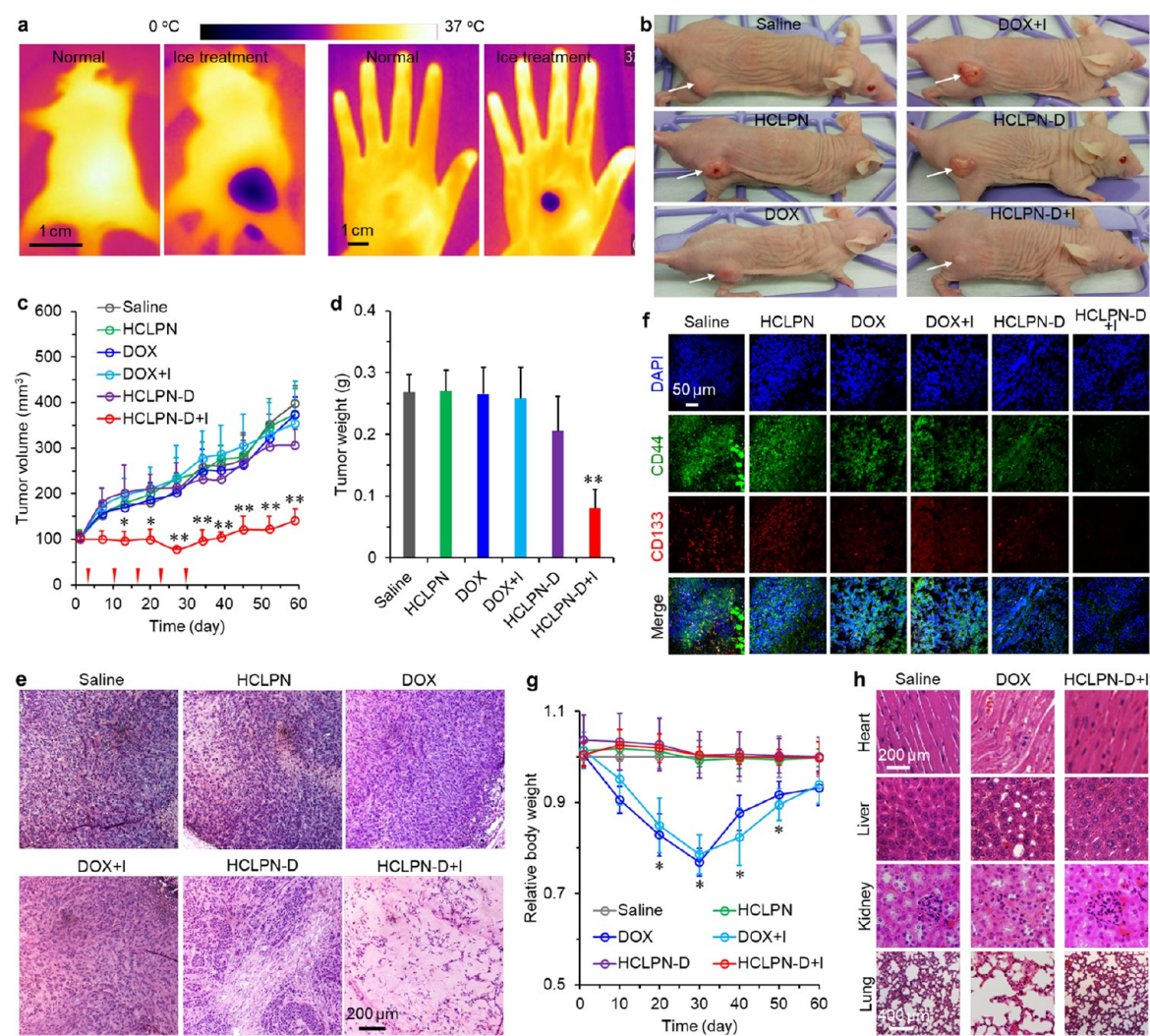
Figure 6. *In vivo* antitumor capacity of HCLPN-D nanoparticles with ice cooling studied using subcutaneous tumor model. (a) Near infrared thermographs of whole animal and human hand before and after ice cooling for 10 min (+I), showing temperature in the region with cooling can be effectively decreased to ∼0 °C. (b) Typical photographs showing the size of tumors (indicated by arrows) on day 59 in mice with six different treatments. (c) Tumor growth curves for the six different treatments. Error bars represent SD ($n = 5$). The red arrow heads indicate the times of conducting injections. *: $p < 0.05$, **: $p < 0.01$ (Kruskal−Wallis H test). (d) Weight of the tumors collected after sacrificing the mice on day 59. Error bars represent SD ($n = 5$). **: $p < 0.01$ (Kruskal−Wallis H test). (e) Representative histology (H&E) images of the tumors collected on day 59. The HCLPN-D+I treated tumors are more necrotic than tumors with the other five treatments. (f) Immunofluorescent staining of CD44 and CD133 in tumor showing diminished expression of both CD44 and CD133 after the treatment with HCLPN-D+I. (g) Body weight and (h) representative micrographs of H&E staining of four important organs with various treatments showing the minimized systemic toxicity of HCLPN-D+I compared to treatments with free DOX (DOX and DOX+I).

imaging, various organs were harvested for *ex vivo* imaging to check the distribution of ICG fluorescence after sacrificing the mice at 9 h. As shown in Figure 5b, only the tumors from mice treated with HCLPN-G nanoparticles has ICG fluorescence with an exposure time of 3 s, which is consistent with the whole-animal imaging data. This is probably due to the enhanced permeability and retention (EPR) effect of tumor vasculature compared to that of normal organs, together with the capability of HA on the surface of the HCLPN-D nanoparticles in targeting CD44 overexpressed on the cancer cells and CSCs.[57,58]

To quantify the biodistribution of ICG fluorescence in the various organs including tumors, the total ICG fluorescence of free ICG and ICG-laden HCLPN-G nanoparticles used for injection into each mouse were obtained. This was done by diluting the 100 μL of free ICG and ICG-laden HCLPN-G

nanoparticles (prepared in the same way as the 100 μL of samples used for injection into each mouse) into 400 μL (to prevent fluorescence overflow) in a centrifuge tube and imaging in the same way as that for both *in vivo* and *ex vivo* imaging. This experiment was conducted in triplicates (Figure 5c). Interestingly, the average total fluorescence of HCLPN-G nanoparticles used for injection into each animal is ∼99% of that of free ICG, indicating minimal quenching of the ICG fluorescence in the nanoparticles. The total fluorescence in each organ shown in Figure 5b was subtracted with the total fluorescence of the corresponding organ from the saline group (to correct any auto fluorescence from tissue). The corrected total fluorescence of ICG in each organ from the free ICG (or HCLPN-G nanoparticles) group shown in Figure 5b was then divided by the average total fluorescence of free ICG (or HCLPN-G nanoparticles) used for injection into each animal
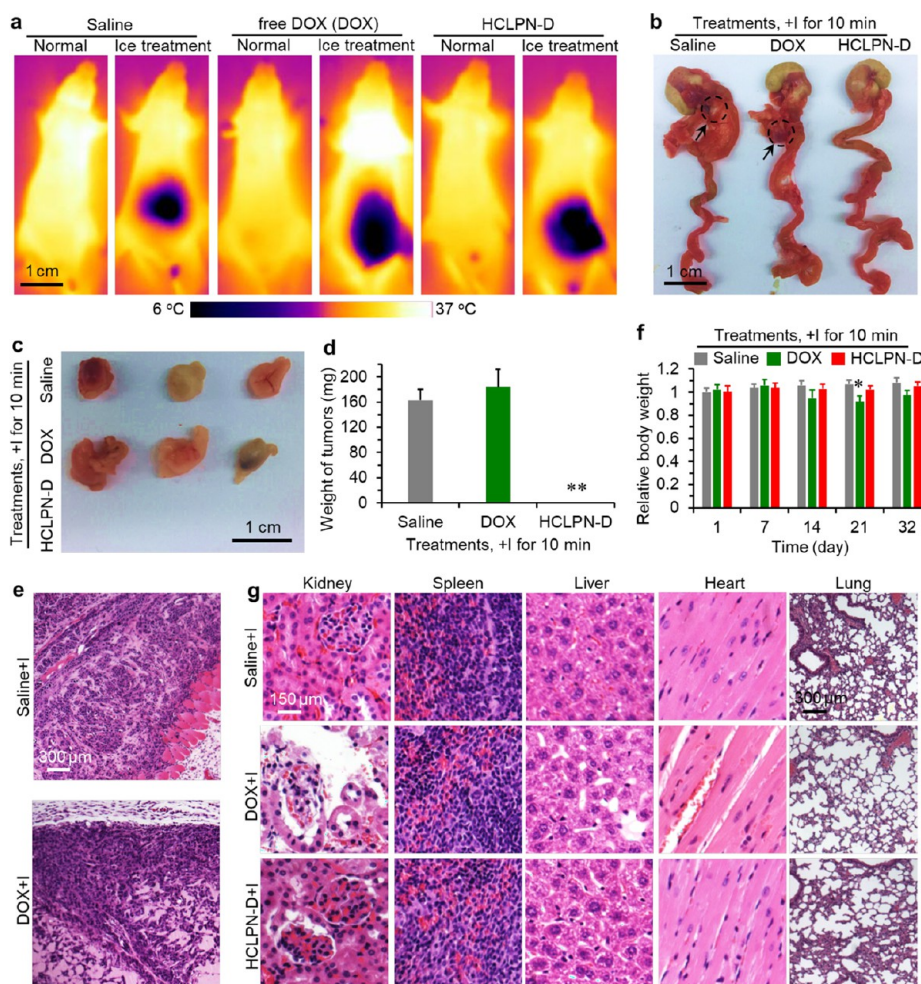
Figure 7. *In viv*o antitumor capacity of HCLPN-D nanoparticles with ice cooling studied using orthotopic metastasis model of ovarian cancer. (a) Near infrared thermographs of whole animal on the ventral side before and after ice cooling for 10 min. The data show that temperature on the skin with cooling on the ventral side of the peritoneal cavity can be effectively decreased to ∼6−10 °C. (b) Photographs showing the typical *in situ* locations of tumors (indicated by arrows and circles) from mice treated with saline and free DOX. (c) Photograph showing the size of tumors collected after sacrificing the mice on day 32 with three different treatments. (d) Weight of the tumors collected on day 32. Error bars represent SD (*n* = 3). (e) Representative histology (H&E) images of the tumors collected on day 32. (f−g) Body weight (f) and representative micrographs of H&E staining of five critical organs (g) with various treatments. The data show reduced systemic toxicity of the treatment of HCLPN-D nanoparticles with ice cooling for 10 min (HCLPN-D+I) compared with the free DOX+I treatment. *: *p* < 0.05 (Kruskal−Wallis *H* test).

(Figure 5c) and averaged, to obtain the percentage of ICG distribution in each organ. As shown in Figure 5d, the accumulation of ICG in tumors is significantly improved by ∼50 times (∼15% versus ∼0.3%) with the nanoparticle encapsulation. This further confirms the observations from the qualitative *in vivo* and *ex vivo* imaging.

Lastly, we treated the drug-resistant tumor-bearing mice with different drug formulations to understand the safety and efficacy of the HCLPN-D nanoparticles in combination with 10 min of ice cooling for overcoming cancer drug resistance. To assess the cooling effect *in vivo*, ice was applied through the skin over the tumor area. FLIR near-infrared thermography was used to determine the temperature immediately after ice cooling (Figure 6a). After 10 min of cooling, the temperature in the tumor area decreases to 4−7 °C. The ice cooling treatment is also efficient on human (hand, Figure 6a). The drug-resistant tumor-bearing mice were randomly divided into six groups: saline, blank nanoparticles (HCLPN), free DOX without or with ice cooling (DOX or DOX+I), and HCLPN-D nanoparticles without or with ice treatment (HCLPN-D or HCLPN-

D+I). Mice were treated with the various formations at a total DOX dose of 3 mg/kg body weight via intravenous injection when the tumor reached ∼100 mm³ on day 1, 8, 15, 22, and 29. After 12 h of each of the injections, tumors were cooled with ice for 10 min. No mice died during the course of the 59 days of treatment and observation.

As shown in Figure 6b,c, tumor growth for treatments with blank HCLPN nanoparticles and free DOX is similar to that of saline control. This is not surprising as the tumors are generated with multidrug-resistant and CSC-enriched cancer cells. In addition, ice cooling does not affect the antitumor ability of free DOX. The tumor volume for the treatment with HCLPN-D is slightly reduced compared to saline control although the difference is not significant. Importantly, the HCLPN-D nanoparticles with ice cooling (HCLPN-D+I) exhibit excellent antitumor capacity and significantly inhibit the tumor growth compared to all the other five treatments. The size and weight of the tumors for the HCLPN-D+I treatment are significantly less than that from all the other five treatments (Figure 6d and Figure S29). Moreover, histological
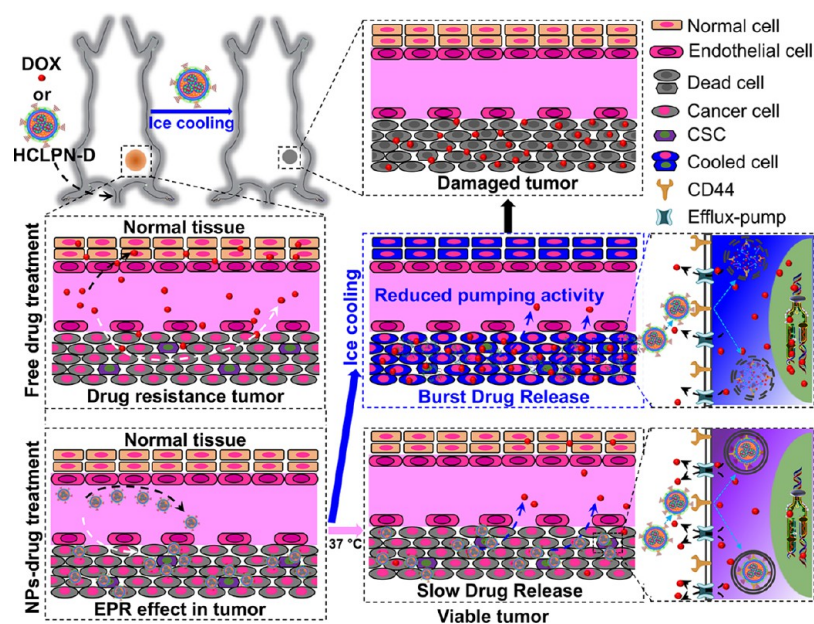
Figure 8. A Schematic illustration of overcoming drug resistance with HCLPN-D nanoparticles and ice cooling for enhanced cancer therapy. *In vivo* accumulation of HCLPN-D nanoparticles in tumor through the enhanced permeability and retention (EPR) effect of tumor vasculature could minimize the side effects associated with free DOX. Moreover, the HCLPN-D nanoparticles can specifically target cancer stem cells (CSCs) via the HA-CD44 interaction to facilitate their uptake by the CSCs. Although drug slowly released from nanoparticles at 37 °C (or mild hyperthermic temperatures) could be still pumped out of the multidrug-resistant cancer cells, the cold-triggered burst drug release together with the compromised pumping activity of membrane transporters in the multidrug-resistant cancer cells under cold temperature could efficiently overcome their drug-resistant capacity. As a result, the cold-responsive nanoparticle in combination with ice cooling could efficiently inhibit the growth of multidrug-resistant tumor *in vivo*.

examination (hematoxylin&eosin or H&E stain) reveals extensive necrosis in the tumors from the HCLPN-D+I treatment group while tumors from all the other groups are more viable (Figure 6e and Figure S30).

CD44 and CD133 are two surface markers involved in many cell functions and believed to be associated with tumor-igenicity.[47,48,53] Both have been commonly used as the surface markers of various CSCs.[47,48,53] We checked the expression of both markers in 2D cultured NCI/RES-ADR cells and 3D-cultured CSC-enriched spheres first. As shown in Figures S31 (for 2D cultured NCI/RES-ADR cells) and S32 (for the CSC-enriched spheres), the expression of CD44 and CD133 in the CSC-enriched spheres is increased compared with 2D cultured NCI/RES-ADR cells. After treatment with HCLPN-D nano-particles for 12 h without ice cooling, the expression of CD44 and CD 133 is decreased only slightly. Importantly, after ice cooling and further incubation for 12 h at 37 °C, the expression of both markers is minimized in both 2D cultured NCI/RES-ADR cells and 3D cultured CSC-enriched spheres (Figure S31−32). In order to check the anti-CSC ability of the HCLPN-D nanoparticles with 10 min of ice cooling *in vivo*, the expression of the variant CD44 and CD133 was further studied in the *in vivo* tumors after the various treatments. Typical micrographs of immunofluorescent staining of the two CSC markers are shown in Figure 6f. The expression of the two markers in tumors treated with saline, HCLPN nanoparticles, DOX, DOX+I, and HCLPN-D nanoparticles is high. In contrast, their expression in tumors with the HCLPN-D+I treatment is negligible. These observations from the immuno-fluorescent staining were further confirmed by immunohisto-chemistry staining of the two markers in tumors from the various treatments (Figure S33), which suggests that the HCLPN-D nanoparticles combined with 10 min of ice cooling

are effective to kill the CSCs *in vivo*. Collectively, these data demonstrate the enhanced *in vivo* antitumor efficacy of the HCLPN-D nanoparticles combined with ice cooling.

Equally important, we did not notice any obvious sign of side effects for the HCLPN-D+I treatment. Although during the ice treatment, normal tissue around tumor might be affected by ice cooling and DOX released from nanoparticles, neither death nor significant drop of body weight was noted for saline, HCLPN nanoparticles, HCLPN-D, and HCLPN-D+I treat-ments (Figure 6g). In contrast, the body weight of mice treated with free DOX and DOX+I were significantly reduced during the treatments, indicating significant systemic toxicity of the treatments with the free drug. To further confirm this, various critical organs including liver, kidney, heart, and lung from saline, DOX, and HCLPN-D+I treatments were harvested, fixed, and assessed by histology (H&E stain). As shown in Figure 6h and Figure S34, free DOX treatment results in hepatic damage including macro- and microvesicular steatosis and bile stasis. Slight nephrotoxicity and cellular damage (vacuolization) of cardiac muscle were also observable for the free DOX treatment. Severe pulmonary damage with markedly reduced alveolar surface area (honeycomb lung) was obvious in the lung of mice with free DOX treatment. However, no obvious damage to these organs was observable in the H&E stained tissue slices for the mice with HCLPN-D+I treatment (Figure 6h and Figure S34).

In order to further confirm the antitumor capacity and safety of the HCLPN-D nanoparticles with ice cooling, an orthotopic metastasis model of ovarian cancer was established by intraperitoneal injection of the NCI/RES-ADR cells into the peritoneal cavity of mice. The mice were then treated with saline, free DOX, and HCLPN-D nanoparticles at a total DOX dose of 3 mg/kg body weight via intraperitoneal injection on

day 7, 14, and 21. After 12 h of each of the injections, tumors (if any) were cooled by applying ice for 10 min on the skin outside the peritoneal cavity on the ventral side. As shown in Figure 7a, the temperature decreased to 6−10 °C at the ice treated area after the 10 min of ice cooling. All the mice were sacrificed on day 32, and tumors can only be found in the saline and free DOX treated mice (Figure 7b-d). The tumors are further confirmed by H&E staining data (Figure 7e). This is not surprising as the NCI/RES-ADR cells are resistant to free DOX, which can be overcome by using HCLPN-D nanoparticles with ice cooling. The body weight of mice treated with free DOX is also reduced and significantly different from that of mice in the saline and HCLPN-D groups on day 21 (Figure 7f).

H&E staining of various critical organs (kidney, spleen, liver, heart, and lung) indicates that the free DOX treatment causes severe kidney injury together with some hepatic and cardiac damage (Figure 7g and Figure S35). The severe renal injury may be because of the intraperitoneal injection free DOX that could diffuse into the organ. Importantly, these side effects of free DOX can be minimized by encapsulating the drug inside HCLPN nanoparticles for delivery via intraperitoneal injection. To further support this, we incubated noncancerous human umbilical vein endothelial cells (HUVECs) with both free DOX and HCLPN-D nanoparticles. As shown in Figure S36, free DOX can easily enter HUVECs but not the NCI/RES-ADR cells (top panels). In contrast, uptake of HCLPN-D nanoparticles by the HUVECs is minimal compared to the NCI/RES-ADR cells either without (middle panels) or with (bottom panels) ice cooling. These data indicate the HCLPN nanoparticles are capable of not only significantly enhancing the efficacy of DOX in destroying drug-resistant tumors when combined with ice cooling, but also minimizing its systemic toxicity via intraperitoneal or intravenous injection.

■ DISCUSSION

In this study, we developed a cold responsive nanoparticle for overcoming the drug resistance of NCI/RES-ADR cells and reducing the potential side effects associated with chemotherapy drug (DOX). As schematically illustrated in Figure 8, there are two possible mechanisms for this strategy to overcome cancer drug resistance. The first mechanism is the ice cooling induced burst release of drug from the HCLPN-D nanoparticles. As shown in Figure 2b, more than 70% of DOX can be released from the HCLPN-D nanoparticles during ice cooling for 5 min. The released free DOX can diffuse out of the endo-/lysosomes driven by its concentration gradient without the need of any metabolic energy. At the same time, the structure of endo-/lysosomes may be damaged during the disassembly of the HCLPN-D nanoparticles as a result of ice cooling (Figure 4c), to further facilitate the escape of the released DOX from the endo/lysosomes. With a large amount of free DOX being released into cytoplasm in a short time, a significant amount of free DOX could bind with its target before being pumped out of the cells by the efflux pumps on the cell membrane (Figures 3, S7, S12, S15−S18, S21, S31, and S32). In contrast, only ∼2.2% of the drug encapsulated in the nanoparticles could be released in 5 h at 37 °C (Figure 2b). This slowly released drug from the nanoparticles could be easily pumped out of the cells by the efflux pump before entering the nuclei (Figures 3, S7, S12, S15−S18, S21, S31, and S32). This mechanism is further supported by the cell viability data showing that ice cooling could greatly and significantly improve the toxicity of the HCLPN-D nanoparticles to the multidrug-

resistant NCI/RES-ADR cells (Figure 4a,b). The second mechanism is that the activity of efflux pumps can be reduced during the ice cooling process. This is supported by the data on cell uptake of free DOX without and with ice cooling (Figures S24 and S25) and the viability data of cells treated by free DOX at high concentrations (50−160 μg/mL) without and with ice cooling (Figures 4a,b and S26). These high concentrations of DOX are relevant because the intracellular concentration of DOX delivered with the HCLPN-D nanoparticles (extracellular DOX: 10 μg/mL) could be this high according to the intracellular fluorescence intensity of DOX (Figure S24 versus Figure 3a). This mechanism is due to the minimized metabolic activity of cells at ice-cold temperature to deprive the energy supply to the efflux pumps that work against the concentration gradient of the chemotherapy drug across the cell membrane (i.e., the drug concentration outside the multidrug-resistant cells is higher than that inside the cells). Furthermore, the HCLPN-D nanoparticles could efficiently and selectively accumulate in tumors compared with free drug (Figure 5), which could carry the chemotherapy drug selectively into tumor. This together with the minimal release of drug from the nanoparticles in normal tissue (always at 37 °C, Figure 2b) can reduce the potential side effects of chemotherapy drug to normal organs in vivo (Figures 6 and 7). We tested this strategy for overcoming cancer multidrug resistance using both the 2D cultured NCI/RES-ADR multidrug-resistant cancer cells and their spheres enriched with CSCs.

The aforementioned two mechanisms for overcoming cancer drug resistance with the HCLPN-D nanoparticles and ice cooling are further supported by data obtained with the drug-resistant A2780ADR ovarian cancer cells. As shown in Figure S37, no red fluorescence of DOX is observable in the A2780ADR cells after incubating them with free DOX (10 μg/mL) at 37 °C for 3 h, followed by either continuously incubating at 37 °C or cooling with ice for 10 min. In stark contrast, red fluorescence of DOX is observable in the cells incubated with the HCLPN-D nanoparticles (containing 10 μg/mL DOX) at 37 °C for 3 h, although the DOX fluorescence is predominantly distributed in the cytosol. Importantly, DOX is located in the nuclei of the cells treated with HCLPN-D nanoparticles with 10 min of cooling with ice after the 3 h of incubation at 37 °C, while almost all DOX is still distributed in the cytosol if the cells are continuously cultured at 37 °C for 10 min more. Quantitative analyses indicate that the intensity of DOX in the cell nuclei is significantly increased after ice cooling, as shown in Figure S38. We further investigated the cell viability of the A2780ADR cells treated with free DOX and HCLPN-D nanoparticles with or without ice cooling for 10 min. As shown in Figure S39, the cytotoxicity of HCLPN-D nanoparticles is significantly enhanced after ice cooling, which is in accordance with the data on cellular uptake shown in Figures S37 and S38 and discussed above. We also noticed that ice cooling for 10 min could further significantly decrease the viability of A2780ADR cells treated with free DOX at 50 μg/mL ($p < 0.05$), which is consistent with the viability data of the NCI/RES-ADR cells with the same treatment (Figure 4a). This is probably due to the second mechanism via reducing the activity of the membrane transporters, as aforementioned for the NCI/RES-ADR cells (Figures S24−S26). This is further confirmed by incubating the A2780ADR cells with free DOX (10 μg/mL) on ice for 1 h. As shown in Figure S40, more free DOX could enter the cells compared with 10 min of ice cooling (Figure S37). This supports that ice cooling could decrease the

activity of the efflux pump (i.e., temperature-dependent activity of the pump), which could minimize the amount of drug (burst-released from the HCLPN-D nanoparticles inside the drug-resistant cells in response to ice cooling) to be pumped out of the cells before it enters the cell nuclei.

Since the HCLPN-D nanoparticles disassemble at ∼10 °C, and biological tissues and cells may become frozen (i.e., form solid ice) with minimized diffusion coefficient for small molecules including chemotherapy drugs below ∼0 °C, the therapeutic temperature with the HCLPN-D nanoparticles for burst drug release to destroy tumors is suggested to be ∼0−10 °C. This can be conveniently achieved by cooling with ice that is readily available in nearly all clinic settings, without the need of a complex refrigeration system to achieve subzero or freezing temperatures. It is worth noting the HCLPN-D nanoparticles are also applicable for applications requiring subzero temperatures. This is because they may disassemble to induce burst drug release during cooling or warming between the subzero temperatures and 37 °C (body temperature). In fact, the temperature is not constant (i.e., decreases with time from 37 °C to ∼4−0 °C) during ice cooling in this study (Figures S8, S9, and S22). Therefore, we compared the viability and DOX distribution in cells treated with free DOX and HCLPN-D nanoparticles under two conditions: at body temperature (37 °C) and with ice cooling to cold temperature (below 10 °C). Our data show the combination of the HCLPN-D nanoparticles and ice cooling could overcome cancer resistance (Figure 3) to effectively kill the multidrug-resistant cells in vitro (Figure 4) and in vivo (Figures 6 and 7).

It is worth noting that the CSC-enriched spheres are derived from NCI/RES-ADR cells and can be maintained only in in vitro culture using ultra low attachment plate and CSC medium. After injection in vivo, some of the cells from the spheres may differentiate, and some of them may remain undifferentiated. In other words, we have no control of the stemness of the cells from the CSC-enriched spheres in vivo. Therefore, the difference between NCI/RES-ADR cells and CSC-enriched spheres with different treatments was studied in vitro, and overall the CSC-enriched spheres are more resistant to drug than 2D cultured NCI/RES-ADR cells (Figure 4a,b). In view of the latter, we used cells from the CSC-enriched spheres to produce tumors for our in vivo studies to investigate if the HCLPN-D nanoparticles with ice cooling could overcome cancer drug resistance in vivo. We do not intend to compare the NCI/RES-ADR cells and CSC-enriched spheres in vivo since we could not control the stemness of the cells in vivo.

We tested the strategy of overcoming cancer drug resistance with the HCLPN-D nanoparticles and ice cooling using both subcutaneous and orthotopic metastasis model of ovarian cancer. For the orthotopic metastasis model, the cells from the CSC-enriched spheres were injected into the peritoneal cavity (where ovarian cancer cells usually metastasize to)[59] of mice via intraperitoneal injection. Consistent with the clinical practice of treating ovarian cancer metastasis,[60] we used intraperitoneal injection to deliver the HCLPN-D nanoparticles for treating the orthotopic metastasis model in this study. In other words, the nanoparticles are delivered into the peritoneal cavity where the tumors are. This may be the major factor that contributes to the excellent therapeutic outcome of the treatment with the HCLPN-D nanoparticles and ice cooling for the orthotopic metastasis model (no tumor was identifiable, Figure 7c), compared with the subcutaneous model (small tumors could be seen, Figure S29). For the latter, the nanoparticles are injected

intravenously through the tail vein that is away from the subcutaneous tumors and the nanoparticles are diluted in blood before reaching the subcutaneous tumors.

In this study, the potential of the proposed strategy of using the cold-responsive nanoparticles for overcoming cancer drug resistance is demonstrated by ice cooling of subcutaneous and intraperitoneal tumors in small animals. Admittedly, ice cooling may be difficult to apply for tumors in deep internal organs (e.g., kidney and liver). Nonetheless, catheters with lumens perfused with cold saline have been widely used for local delivery of cold into deep organs to achieve local hypothermia with the aid of minimally invasive surgical technologies such as thoracoscopy, laparoscopy, and endoscopy.[61−63] Therefore, the local delivery of cold required for the nanoparticle system developed in this study is not a hurdle to its future potential applications for destroying tumors in deep organs. Since techniques using cold and freezing temperatures have been widely studied and used for treating various diseases including cancer in the clinic (known as cryosurgery, cryotherapy, cryoablation, and hypothermia),[28−34] our cold responsive nanoparticle-mediated drug delivery may be combined with these techniques to further improve their safety and efficacy of treating various diseases including cancer.

CONCLUSIONS

We developed a cold-responsive hybrid HCLPN-D nanoparticle composed of HA, chitosan, DPPC, PNIPAM-B, and PF127 for targeted delivery of chemotherapeutics (DOX) into multidrug-resistant cancer cells and their CSCs in vitro and multidrug-resistant tumors in vivo. The HCLPN-D nanoparticles could significantly improve drug delivery into tumors through the EPR effect of tumor vasculature after intravenous injection into the tail vein (Figure 8). Moreover, the HCLPN-D nanoparticles could quickly and irreversibly disassemble at cold temperatures (<12 °C), which can induce burst release of most encapsulated drug from the nanoparticles. Moreover, the cold-triggered burst release of DOX together with the cold temperature per se (to reduce the activity of membrane transporters) can efficiently overcome the multidrug-resistant capacity of NCI/RES-ADR cells (Figure 8). Furthermore, CSCs enriched spheres derived from the multidrug-resistant cancer cells were used to account for the multifaceted mechanisms of cancer drug resistance. Our extensive in vitro studies with both 2D cultured multidrug-resistant cells and 3D microscale tumors (i.e., spheres) enriched with multidrug-resistant CSCs as well as in vivo studies using the CSC-derived tumors grown in mice, demonstrate the great potential of the HCLPN-D nanoparticles with ice cooling for overcoming different mechanisms associated with cancer multidrug resistance for effective and safe cancer therapy.

ASSOCIATED CONTENT

ⓈSupporting Information

The Supporting Information is available free of charge on the ACS Publications website at DOI: 10.1021/acscentsci.8b00050.

Experimental details of preparation of nanoparticles, drug encapsulation and release, in vitro cell imaging and cell viability, flow cytometry, TEM imaging of cell, in vivo animal study and immunohistochemical staining. Supporting Figures S1−S40 (PDF)

■ AUTHOR INFORMATION

Corresponding Author

*E-mail: shawnhe@umd.edu.

ORCID ⊙

Gang Zhao: 0000-0002-0201-1825

Xiaoming He: 0000-0003-0125-6086

Notes

CMJ is an employee of the Maryland Veterans Affairs (VA) Health Care Systems at the Baltimore VA Medcial Center.

The authors declare the following competing financial interest(s): The views reported in this paper do not reflect the views of the Department of Veterans Affairs or the United States Government. CMJ has an equity position in Cellth LLC. All other authors declare no competing financial interest.

■ REFERENCES

(1) Gottesman, M. M.; Fojo, T.; Bates, S. E. Multidrug resistance in cancer: role of ATP-dependent transporters. *Nat. Rev. Cancer* **2002**, *2*, 48−58.

(2) Szakács, G.; Paterson, J. K.; Ludwig, J. A.; Booth-Genthe, C.; Gottesman, M. M. Targeting multidrug resistance in cancer. *Nat. Rev. Drug Discovery* **2006**, *5*, 219−234.

(3) Rubbia-Brandt, L.; Audard, V.; Sartoretti, P.; Roth, A.; Brezault, C.; Le Charpentier, M.; Dousset, B.; Morel, P.; Soubrane, O.; Chaussade, S. Severe hepatic sinusoidal obstruction associated with oxaliplatin-based chemotherapy in patients with metastatic colorectal cancer. *Ann. Oncol.* **2004**, *15*, 460−466.

(4) Modok, S.; Mellor, H. R.; Callaghan, R. Modulation of multidrug resistance efflux pump activity to overcome chemoresistance in cancer. *Curr. Opin. Pharmacol.* **2006**, *6*, 350−354.

(5) Aller, S. G.; Yu, J.; Ward, A.; Weng, Y.; Chittaboina, S.; Zhuo, R.; Harrell, P. M.; Trinh, Y. T.; Zhang, Q.; Urbatsch, I. L.; Chang, G. Structure of P-glycoprotein reveals a molecular basis for poly-specific drug binding. *Science* **2009**, *323*, 1718−1722.

(6) Kabanov, A. V.; Batrakova, E. V.; Alakhov, V. Y. Pluronic block copolymers for overcoming drug resistance in cancer. *Adv. Drug Delivery Rev.* **2002**, *54*, 759−779.

(7) Wang, H.; Gao, Z.; Liu, X.; Agarwal, P.; Zhao, S.; Conroy, D. W.; Ji, G.; Yu, J.; Jaroniec, C. P.; Liu, Z.; Lu, X.; Li, X.; He, X. Targeted production of reactive oxygen species in mitochondria to overcome cancer drug resistance. *Nat. Commun.* **2018**, *9*, 562.

(8) Gottesman, M. M. Mechanisms of cancer drug resistance. *Annu. Rev. Med.* **2002**, *53*, 615−627.

(9) Donnenberg, V. S.; Donnenberg, A. D. Multiple drug resistance in cancer revisited: the cancer stem cell hypothesis. *J. Clin. Pharmacol.* **2005**, *45*, 872−877.

(10) Singh, A.; Settleman, J. EMT, cancer stem cells and drug resistance: an emerging axis of evil in the war on cancer. *Oncogene* **2010**, *29*, 4741−4751.

(11) Dean, M.; Fojo, T.; Bates, S. Tumour stem cells and drug resistance. *Nat. Rev. Cancer* **2005**, *5*, 275−284.

(12) Dallas, N. A.; Xia, L.; Fan, F.; Gray, M. J.; Gaur, P.; van Buren, G., 2nd; Samuel, S.; Kim, M. P.; Lim, S. J.; Ellis, L. M. Chemoresistant colorectal cancer cells, the cancer stem cell phenotype, and increased sensitivity to insulin-like growth factor-I receptor inhibition. *Cancer Res.* **2009**, *69*, 1951−1957.

(13) Clarke, M. F.; Dick, J. E.; Dirks, P. B.; Eaves, C. J.; Jamieson, C. H.; Jones, D. L.; Visvader, J.; Weissman, I. L.; Wahl, G. M. Cancer stem cells—perspectives on current status and future directions: AACR Workshop on cancer stem cells. *Cancer Res.* **2006**, *66*, 9339−9344.

(14) Clevers, H. The cancer stem cell: premises, promises and challenges. *Nat. Med.* **2011**, 313−319.

(15) Zhou, J.; Zhang, Y. Preclinical development of cancer stem cell drugs. *Expert Opin. Drug Discovery* **2009**, *4*, 741−752.

(16) Lou, H.; Dean, M. Targeted therapy for cancer stem cells: the patched pathway and ABC transporters. *Oncogene* **2007**, *26*, 1357−1360.

(17) Maugeri-Saccà, M.; Vigneri, P.; De Maria, R. Cancer stem cells and chemosensitivity. *Clin. Cancer Res.* **2011**, *17*, 4942−4947.

(18) Peer, D.; Karp, J. M.; Hong, S.; Farokhzad, O. C.; Margalit, R.; Langer, R. Nanocarriers as an emerging platform for cancer therapy. *Nat. Nanotechnol.* **2007**, *2*, 751−760.

(19) Cho, K.; Wang, X.; Nie, S.; Shin, D. M.; Chen, Z. Therapeutic nanoparticles for drug delivery in cancer. *Clin. Cancer Res.* **2008**, *14*, 1310−1316.

(20) Allen, T. M.; Cullis, P. R. Drug delivery systems: entering the mainstream. *Science* **2004**, *303*, 1818−1822.

(21) Sykes, E. A.; Chen, J.; Zheng, G.; Chan, W. C. Investigating the impact of nanoparticle size on active and passive tumor targeting efficiency. *ACS Nano* **2014**, *8*, 5696−5706.

(22) Nguyen, H. V.-T.; Chen, Q.; Paletta, J. T.; Harvey, P.; Jiang, Y.; Zhang, H.; Boska, M. D.; Ottaviani, M. F.; Jasanoff, A.; Rajca, A.; Johnson, J. Nitroxide-Based Macromolecular Contrast Agents with Unprecedented Transverse Relaxivity and Stability for Magnetic Resonance Imaging of Tumors. *ACS Cent. Sci.* **2017**, *3*, 800−811.

(23) Davis, M. E.; Shin, D. M.; Chen, Z. Nanoparticle therapeutics: an emerging treatment modality for cancer. *Nat. Rev. Drug Discovery* **2008**, *7*, 771−782.

(24) Motornov, M.; Roiter, Y.; Tokarev, I.; Minko, S. Stimuli-responsive nanoparticles, nanogels and capsules for integrated multifunctional intelligent systems. *Prog. Polym. Sci.* **2010**, *35*, 174−211.

(25) Xia, H.; Li, F.; Hu, X.; Park, W.; Wang, S.; Jang, Y.; Du, Y.; Baik, S.; Cho, S.; Kang, T.; Kim, D.-H.; Ling, D.; Hui, K. M.; Hyeon, T. pH-Sensitive Pt Nanocluster Assembly Overcomes Cisplatin Resistance and Heterogeneous Stemness of Hepatocellular Carcinoma. *ACS Cent. Sci.* **2016**, *2*, 802−811.

(26) Schmaljohann, D. Thermo-and pH-responsive polymers in drug delivery. *Adv. Drug Delivery Rev.* **2006**, *58*, 1655−1670.

(27) Gao, W.; Chan, J.; Farokhzad, O. C. pH-responsive nano-particles for drug delivery. *Mol. Pharmaceutics* **2010**, *7*, 1913−1920.

(28) Rubinsky, B. Cryosurgery. *Annu. Rev. Biomed. Eng.* **2000**, *2*, 157−187.

(29) Gage, A.; Baust, J.; Baust, J. Experimental cryosurgery investigations *in vivo*. *Cryobiology* **2009**, *59*, 229−243.

(30) Gage, A. A. Cryosurgery in the treatment of cancer. *Surg. Gynecol. Obstet.* **1992**, *174*, 73−92.

(31) Avitall, B.; Kalinski, A. Cryotherapy of cardiac arrhythmia: From basic science to the bedside. *Heart Rhythm* **2015**, *12*, 2195−2203.

(32) Villablanca, P. A.; Rao, G.; Briceno, D. F.; Lombardo, M.; Ramakrishna, H.; Bortnick, A.; Garcia, M.; Menegus, M.; Sims, D.; Makkiya, M.; Mookadam, F. Therapeutic hypothermia in ST elevation myocardial infarction: a systematic review and meta-analysis of randomised control trials. *Heart* **2016**, *102*, 712−719.

(33) Hoffmann, N. E.; Bischof, J. C. The cryobiology of cryosurgical injury. *Urology* **2002**, *60*, 40−49.

(34) Pilcher, T. A.; Saul, J. P.; Hlavacek, A. M.; Haemmerich, D. Contrasting effects of convective flow on catheter ablation lesion size: cryo versus radiofrequency energy. *Pacing Clin. Electrophysiol.* **2008**, *31*, 300−307.

(35) Zhang, W.; Gilstrap, K.; Wu, L.; Bahadur K. C., R.; Moss, M. A.; Wang, Q.; Lu, X.; He, X. Synthesis and characterization of thermally responsive Pluronic F127-chitosan nanocapsules for controlled release and intracellular delivery of small molecules. *ACS Nano* **2010**, *4*, 6747−6759.

(36) Lee, S. H.; Choi, S. H.; Kim, S. H.; Park, T. G. Thermally sensitive cationic polymer nanocapsules for specific cytosolic delivery and efficient gene silencing of siRNA: swelling induced physical disruption of endosome by cold shock. *J. Controlled Release* **2008**, *125*, 25−32.

(37) Yang, Z.; Cheng, Q.; Jiang, Q.; Deng, L.; Liang, Z.; Dong, A. Thermo-sensitive nanoparticles for triggered release of siRNA. *J. Biomater. Sci., Polym. Ed.* **2015**, *26*, 264−276.

(38) Ward, M. A.; Georgiou, T. K. Thermoresponsive polymers for biomedical applications. *Polymers* **2011**, *3*, 1215−1242.

(39) Gan, J.; Guan, X.; Zheng, J.; Guo, H.; Wu, K.; Liang, L.; Lu, M. Biodegradable, thermoresponsive PNIPAM-based hydrogel scaffolds for the sustained release of levofloxacin. *RSC Adv.* **2016**, *6*, 32967−32978.

(40) Lima, L. H.; Morales, Y.; Cabral, T. Ocular Biocompatibility of Poly-N-Isopropylacrylamide (pNIPAM). *J. Ophthalmol.* **2016**, *2016*, 1−6.

(41) Jung, H. H.; Park, K.; Han, D. K. Preparation of TGF-β1-conjugated biodegradable pluronic F127 hydrogel and its application with adipose-derived stem cells. *J. Controlled Release* **2010**, *147*, 84−91.

(42) Dimitrov, I.; Trzebicka, B.; Müller, A. H.; Dworak, A.; Tsvetanov, C. B. Thermosensitive water-soluble copolymers with doubly responsive reversibly interacting entities. *Prog. Polym. Sci.* **2007**, *32*, 1275−1343.

(43) Wang, H.; Agarwal, P.; Zhao, S.; Yu, J.; Lu, X.; He, X. A Near-Infrared Laser-Activated "Nanobomb" for Breaking the Barriers to MicroRNA Delivery. *Adv. Mater.* **2016**, *28*, 347−355.

(44) Zheng, M.; Yue, C.; Ma, Y.; Gong, P.; Zhao, P.; Zheng, C.; Sheng, Z.; Zhang, P.; Wang, Z.; Cai, L. Single-step assembly of DOX/ICG loaded lipid−polymer nanoparticles for highly effective chemo-photothermal combination therapy. *ACS Nano* **2013**, *7*, 2056−2067.

(45) Wang, H.; Agarwal, P.; Zhao, S.; Xu, R. X.; Yu, J.; Lu, X.; He, X. Hyaluronic acid-decorated dual responsive nanoparticles of Pluronic F127, PLGA, and chitosan for targeted co-delivery of doxorubicin and irinotecan to eliminate cancer stem-like cells. *Biomaterials* **2015**, *72*, 74−89.

(46) Lu, Y.; Hu, Q.; Lin, Y.; Pacardo, D. B.; Wang, C.; Sun, W.; Ligler, F. S.; Dickey, M. D.; Gu, Z. Transformable liquid-metal nanomedicine. *Nat. Commun.* **2015**, *6*, 10066.

(47) Wang, H.; Agarwal, P.; Zhao, S.; Yu, J.; Lu, X.; He, X. Combined cancer therapy with hyaluronan-decorated fullerene-silica multifunctional nanoparticles to target cancer stem-like cells. *Biomaterials* **2016**, *97*, 62−73.

(48) Collins, A. T.; Berry, P. A.; Hyde, C.; Stower, M. J.; Maitland, N. J. Prospective identification of tumorigenic prostate cancer stem cells. *Cancer Res.* **2005**, *65*, 10946−10951.

(49) Trédan, O.; Galmarini, C. M.; Patel, K.; Tannock, I. F. Drug resistance and the solid tumor microenvironment. *J. Natl. Cancer. Inst.* **2007**, *99*, 1441−1454.

(50) Wang, H.; Agarwal, P.; Zhao, S.; Yu, J.; Lu, X.; He, X. A biomimetic hybrid nanoplatform for encapsulation and precisely controlled delivery of theranostic agents. *Nat. Commun.* **2015**, *6*, 10081.

(51) Draffin, J. E.; McFarlane, S.; Hill, A.; Johnston, P. G.; Waugh, D. J. CD44 potentiates the adherence of metastatic prostate and breast cancer cells to bone marrow endothelial cells. *Cancer Res.* **2004**, *64*, 5702−5711.

(52) Bourguignon, L. Y.; Singleton, P. A.; Zhu, H.; Zhou, B. Hyaluronan promotes signaling interaction between CD44 and the transforming growth factor beta receptor I in metastatic breast tumor cells. *J. Biol. Chem.* **2002**, *277*, 39703−39712.

(53) Rao, W.; Wang, H.; Han, J.; Zhao, S.; Dumbleton, J.; Agarwal, P.; Zhang, W.; Zhao, G.; Yu, J.; Zynger, D. L.; Lu, X.; He, X. Chitosan-Decorated Doxorubicin-Encapsulated Nanoparticle Targets and Eliminates Tumor Reinitiating Cancer Stem-Like Cells. *ACS Nano* **2015**, *9*, 5725−5740.

(54) Schinkel, A. H.; Wagenaar, E.; Mol, C. A.; van Deemter, L. P-glycoprotein in the blood-brain barrier of mice influences the brain penetration and pharmacological activity of many drugs. *J. Clin. Invest.* **1996**, *97*, 2517−2524.

(55) Oh, N.; Park, J.-H. Endocytosis and exocytosis of nanoparticles in mammalian cells. *Int. J. Nanomed.* **2014**, *9*, 51−63.

(56) Maxfield, F. R.; McGraw, T. E. Endocytic recycling. *Nat. Rev. Mol. Cell Biol.* **2004**, *5*, 121−132.

(57) Maruyama, K. Intracellular targeting delivery of liposomal drugs to solid tumors based on EPR effects. *Adv. Drug Delivery Rev.* **2011**, *63*, 161−169.

(58) Huo, M.; Wang, L.; Chen, Y.; Shi, J. Tumor-selective catalytic nanomedicine by nanocatalyst delivery. *Nat. Commun.* **2017**, *8*, 357.

(59) Manzotti, C.; Audisio, R. A.; Pratesi, G. Importance of orthotopic implantation for human tumors as model systems: relevance to metastasis and invasion. *Clin. Exp. Metastasis* **1993**, *11*, 5−14.

(60) Agarwal, R.; Kaye, S. B. Ovarian cancer: strategies for overcoming resistance to chemotherapy. *Nat. Rev. Cancer* **2003**, *3*, 502−516.

(61) Cattaneo, G.; Schumacher, M.; Maurer, C.; Wolfertz, J.; Jost, T.; Büchert, M.; Keuler, A.; Boos, L.; Shah, M.; Foerster, K.; Niesen, W.-D.; Ihorst, G.; Urbach, H.; Meckel, S. Endovascular cooling catheter for selective brain hypothermia: an animal feasibility study of cooling performance. *Am. J. Neuroradiol.* **2016**, *37*, 885−891.

(62) Inoue, S.; Mori, A.; Shimizu, H.; Yoshitake, A.; Tashiro, R.; Kabei, N.; Yozu, R. Combined use of an epidural cooling catheter and systemic moderate hypothermia enhances spinal cord protection against ischemic injury in rabbits. *J. Thorac. Cardiovasc. Surg.* **2013**, *146*, 696−701.

(63) Crain, D. S.; Spencer, C. R.; Favata, M. A.; Amling, C. L. Transureteral saline perfusion to obtain renal hypothermia: potential application in laparoscopic partial nephrectomy. *JSLS* **2004**, *8*, 217−222.